Research Square

Preprints are preliminary reports that have not undergone peer review.
They should not be considered conclusive, used to inform clinical practice,
or referenced by the media as validated information.

Three-Dimensional Finite Element Analysis of the Biomechanical Effects of Canine Lingual Bite Ramp on Clear Aligner Therapy in Extraction Cases

jiayi wang
Nanjing Children's Hospital
yiting chu
Nanjing Children's Hospital
yuan zhang
The Affiliated Stomatological Hospital of Nanjing Medical University
kai zheng
The Affiliated Stomatological Hospital of Nanjing Medical University
guoqing li
The Affiliated Stomatological Hospital of Nanjing Medical University
chi zhang
zhangchi1006@njmu.edu.cn

The Affiliated Stomatological Hospital of Nanjing Medical University
zhuang yuan
Nanjing Children's Hospital

Research Article

Keywords: Three-dimensional finite element analysis, Canine distalization, Clear aligner therapy, Bite ramp, Instantaneous center of rotation (ICR)

Posted Date: August 14th, 2026

DOI: https://doi.org/10.21203/rs.3.rs-10418958/v1

License: This work is licensed under a Creative Commons Attribution 4.0 International License.
Read Full License

Additional Declarations: No competing interests reported.

Abstract

Background

To investigate how a canine bite ramp (CBR) in clear aligners affects the three-dimensional displacement of maxillary anterior teeth during canine distalization under different occlusal forces and step sizes, and to provide biomechanical insights for extraction space closure.

Methods

A three-dimensional finite element model including the dentition, periodontal ligament, clear aligner, and CBR was constructed to simulate canine distalization. We designed 20 loading conditions in this experiment, consisting of a combination of 5 bilateral occlusal force levels (0, 50, 100, 150, 200 N, half per canine) and 4 step sizes (0.10, 0.15, 0.20, 0.25 mm). To analyze the stress distribution in the tooth and periodontal tissues, the displacement of the crown and root apex, and the migration behavior of the instantaneous center of rotation (ICR).

Results

Under occlusal loading, the CBR significantly enhanced root control during canine distalization, converting tipping movement into near-bodily translation. This tendency was amplified by higher occlusal loads and smaller step increments. With a 0.10 mm step, synchronous crown–root movement was achieved at forces ranging from 25 to 50 N per canine. In contrast, a large step (0.25 mm) required over 75 N to achieve the same effect. Additionally, occlusal forces resulted in vertical intrusion and mild labial tipping effect on the incisors, and both of which were better constrained when the smaller step was applied.

Conclusion

During canine distalization, CBR effectively stabilizes root control and may serve as a mechanical aid for regulating anterior torque and intrusion. Clinically, it is advisable to apply relatively small step sizes (≤ 0.15 mm) together with moderate occlusal forces (25–50 N per canine) in order to strike a balance between root control efficiency and anterior anchorage preservation.

Introduction

Clear aligners have gained wide acceptance in clinical practice, largely due to their discreet appearance, improved comfort, and relatively predictable outcomes [1]. In complex extraction cases, particularly

those requiring extensive anterior retraction, the biomechanical performance of these devices is still limited by several widely acknowledged constraints [2].

Compared with fixed appliances, clear aligners are less rigid and rely heavily on elastic recovery of the material to close the space. When effective force transmission across the extraction site is lacking, force continuity is lost, which often produces a characteristic “roller coaster” pattern: distal tipping of the canine, lingual inclination and subsequent elongation of the incisors, and mesial rotation of the molars [3-5]. Although staged movement is used, precise root control of the canine is still essential for achieving bodily retraction and preventing bone fenestration [6]. The difficulty of vertical control is amplified in deep overbite cases. Two primary factors have been identified the limited efficiency of incisor intrusion and the bite block effect. The former limits the extent of true intrusion achievable, and the latter reduces the available vertical space for controlled retraction. As a result, those factors restrict space closure and affect both periodontal and esthetic outcomes[7,8].

The lingual bite ramp on the maxillary canine is already used as a clinical strategy for assisting bite opening. Furthermore, current evidence suggests that such a ramp may have some effect on improving torque control and root parallelism during canine distalization. Based on finite element simulations of force application in clear aligner systems the ramp could redirect occlusal forces to influence root torque control [9,10]. Currently, quantitative studies examining the biomechanical effects of the canine bite ramp remain limited.

Therefore, this study aims to investigate whether the lingual bite ramp on the maxillary canine can exert root control during canine distalization under occlusal force in clear aligner treatment, and further analyze the influence of occlusal force magnitude and movement step on mechanical effects, in order to clarify its mechanical mechanism and offer a theoretical basis for clinical design.

Materials and Methods

1.1 Study Subjects

A single male subject with normal occlusion was recruited. Inclusion criteria: (1) Angle Class I molar relationship; (2) presence of permanent dentition with no missing teeth and normal morphology; (3) good dental and periodontal health; (4) absence of systemic diseases; (5) no history of orthodontic treatment; and (6) no significant temporomandibular joint abnormalities. This study was approved by the Ethics Committee of the Affiliated Stomatological Hospital of Nanjing Medical University (Approval No. NKYEC-PJ2023-163-001). Written informed consent was obtained from the patient's legal guardian/parent for the publication of this case report and any accompanying images."

1.2 Finite Element Model Preparation

Cone beam computed tomography (CBCT) was used to scan the volunteer's maxilla. The DICOM data were imported into Mimics software (Materialise Software, Leuven, Belgium) for reconstruction into a

three-dimensional point cloud and generation of an STL model. Geomagic Studio software (Geomagic Company, NC, USA) was used for denoising, hole filling, smoothing, and mesh optimization to obtain a high-quality maxillary dentition model. The periodontal ligament model was generated by expanding 0.2 mm outward from the root surface using Boolean operations [11]; he limitations of the uniform thickness assumption are discussed later.

Using FEBio software (Musculoskeletal Research Laboratories, University of Utah, USA) and incorporating the material properties of clear aligners, a 0.5-mm-thick appliance model was constructed. Distal movement of the canine was simulated in step sizes of 0.10, 0.15, 0.20, and 0.25 mm. A bite ramp guide (base area: 5 × 4 mm^2) was designed in CATIA, attached to the canine, and saved as an STL file after surface optimization. Displacement loading was then applied using a geometric preset displacement combined with a penalty contact algorithm.

The model was iteratively refined until displacement changes were reduced to less than 5%. The final mesh consisted of 10,349 surface nodes, with 4,044 on the canine, 2,950 on the lateral incisor, and 3,355 on the central incisor, discretized using second-order tetrahedral elements (C3D10). The displacement trends of the model were consistent with published literature under comparable conditions[12].

1.3 Material Properties

Based on previous literature [13], all structures are modeled as isotropic, homogeneous, and linearly elastic materials (Table 1). Notably, this simplified assumption characterizes the instantaneous loading response.

Material	Elastic Modulus (MPa)	Poisson's Ratio
Alveolar bone	1.73×10^3	0.30
Tooth	1.96×10^4	0.30
Periodontal ligament	6.82×10^{-2}	0.45
Clear aligner	5.82×10^2	0.36

Table 1. Material Parameters

1.4 Contact and Constraint Conditions

The contact properties among the structural interfaces are defined in FEBio as follows [14]: (1) The appliance-tooth contact is modeled as frictional surface-to-surface contact (μ=0.2); (2) The tooth root–periodontal ligament and periodontal ligament–alveolar bone interfaces are defined as frictionless bonded contacts to simulate physiological adhesion; (3) The maxilla and alveolar bone are subjected to a six-degree-of-freedom fully fixed constraint. This full constraint assumption may overestimate the anchorage stiffness, and its directional influence is analyzed in the discussion. The tooth and

periodontal ligament system remains unconstrained along the X, Y, and Z axes, allowing unrestricted displacement and deformation.

1.5 Establishment of Spatial Coordinate System

The intersection of the palatal suture with the midpoint of the line segment connecting the adjacent contact points of the maxillary first molar and second premolar on both sides serves as the coordinate origin to establish a global three-dimensional coordinate system: X-axis (left-right, positive toward the patient's right), Y-axis (mesiodistal, positive toward the mesial), and Z-axis (vertical, positive upward). Subsequently, a local anatomical coordinate system, where the first principal component (PC1) defines the tooth's long axis, is independently established for each tooth via principal component analysis (PCA). Unlike the global coordinate system, the local coordinate system is employed to mitigate the influence of variations in the initial spatial orientation of teeth on ICR calculations.

1.6 Loading Conditions and Working Condition Design

Two sets of independent variables were established: (1) Displacement increment: 0.10, 0.15, 0.20, 0.25 mm; (2) Total bilateral occlusal force: 0, 50, 100, 150, 200 N (where the unilateral force equals half the total value: 0, 25, 50, 75, 100 N), applied perpendicularly to the bottom surface of the plane guide plate. Twenty loading scenarios were defined by combining these variables (Figure 1).

The applied occlusal force ranged from light occlusion (25 N per side) to maximum clenching (100 N per side). The upper limit of 100 N per side corresponds to the maximum occlusal force reported in adults[15]. In clinical practice, orthodontic patients typically wear the appliance in a passive state, so the actual average occlusal force is lower than the maximum. Accordingly, the force values used in this study represent a parametric exploration of upper boundaries. Clinical application should be individually adjusted.

1.7 Kinematic Analysis and Local Coordinate System Definition

1.7.1 Establishment of Local Coordinate System

To minimize the influence of initial tooth posture on the calculation of the Center of Rotation (CR) [16], a local coordinate system was established for each canine using Principal Component Analysis (PCA). All 4,044 surface nodes per canine tooth were used as input data. We extracted the first principal component (PC1) to represent the long axis of the tooth. The vector orientation was then adjusted via sign correction to ensure its angle with the positive Z-axis was less than 90°. Compared with manual anatomical landmark identification, this method eliminates subjective errors and shows greater robustness against variations in tooth morphology.

1.7.2 Rigid Body Transformation and Rotation Parameter Solving

In orthodontic biomechanics, tooth displacement under varied force systems can be modeled as rigid body motion, that is what we have done in this simulation [17]. We used the Kabsch algorithm to compute the rigid transformation parameters between the pre- and post-displacement positions[18] .

Then we constructed a covariance matrix H = Pcentered^T × Qcentered after aligning the centroids. Singular value decomposition(SVD) of H (H = UΣV^T) yielded the rotation matrix R = VU^T (if det(R) < 0, the third column of V is flipped). This approach follows the standard Kabsch algorithm, which has been employed in previous biomechanical studies for extracting rotation axes from point-cloud data[19]. Next, we performed eigenvalue decomposition of **R**, extracting the eigenvector corresponding to eigenvalue 1, which defines the direction vector of the rotation axis. The rotation angle θ was computed as θ = arccos((tr(**R**) − 1) / 2). To fully determine the axis in space, we applied the Moore–Penrose generalized inverse to the linear system derived from the rigid-body condition, yielding the coordinates of the center of rotation (CR).To mitigate numerical noise, we omitted the ICR calculation when |displacement| < 10^{-7} mm, and **instead performed** the computation on a PCA-reduced point set. By linking CR points across successive force magnitudes under the same loading condition, we generated a migration trajectory that quantitatively captured the dynamic transition from tilt-dominated motion to overall translation.

1.8 Data Processing and Calculation of Biomechanical Indicators

We imported the nodal displacement data from FEBio in batches; these three-dimensional vectors represented the response of roughly 4,000 to 8,000 nodes per loading condition. To build a master database for subsequent analysis, we integrated these displacement data with the initial coordinates of the tooth surface nodes, resulting in a consolidated dataset of 848,618 records. For the 20 loading conditions applied to the cuspid under centric occlusion, we then individually calculated key biomechanical indicators:

1. Crown-Root Displacement Ratio：The ratio of absolute mesiodistal (Y-axis) displacement of reference noded at the crown and root apices. A ratio >1 defines tipping; ≈1, bodily movement; <1, predominant root movement.
2. ICR spatial localization: We used the PCA local coordinate system and the Kabsch rigid transformation algorithm to compute the optimal rotation matrix for the 4,044 surface nodes of each canine. From this rotation matrix, we then extracted the rotation axis direction and the spatial coordinates of the center of rotation, which yielded the projection height h_cr_pca of the ICR onto the tooth long axis (PC1) and the rotation angle θ.
3. The h_cr_pca threshold defined movement types as follows: bodily translation (h > 10 mm), controlled tipping (0 < h ≤ 10 mm), uncontrolled tipping (−2 mm ≤ h ≤ 0), and root movement (h < −2 mm). We set the center of resistance (CRes) at h = −2.0 mm, corresponding to the middle third of the root.

We eliminated initial posture differences by using PCA. For each canine, we computed the optimal rotation matrix via the Kabsch algorithm and SVD. Then we applied the Moore–Penrose generalized

inverse to determine the rotation axis. To mitigate numerical noise, we excluded any rigid body motion below 10^{-7} mm from the ICR analysis.

Results

2.1 Tooth Stress Distribution

As shown in Figure 2, the von Mises stress fields in the maxillary canine were qualitatively similar across loading conditions, with stress hotspots consistently arising at the cervical region of the tooth and the lingual surface of the crown. The shared MPa scale applied to all subplots.

FEA revealed that step size and occlusal force jointly modulated stress distribution. Under external loading (0 N), stresses primarily localized on the lingual crown surface and cervical region. When a vertical occlusal force was applied, the peak stress migrated toward the mid-root and adjacent alveolar crest. As force increased, the high-stress area (warm-color region) expanded, producing a more uniform distribution. This pattern was consistent with the biomechanical resistance during distal movement. Compared with larger movement steps, we observed that smaller steps resulted in a flatter stress gradient and less pronounced local stress concentrations.

2.2 Crown and root apex displacement of central and lateral incisors

To assess load transfer to the anterior segment, we quantified crown and root apex displacements of the maxillary central and lateral incisors—the primary anchorage units. The displacement patterns are summarized in Figure 3. As the applied force increased, the teeth exhibited a primarily vertical intrusion pattern, with the magnitude increasing proportionally. On average, the maxillary central incisors displayed more intrusion than the lateral incisors. And this differential intrusion pattern functionally counteracts the elongation component of the “roller coaster” effect in clear aligner therapy.

By contrast, labial tipping of the incisors reflected a more complex interaction. As established by the occlusal load, tipping increased nonlinearly with displacement magnitude. Specifically, larger step sizes were associated with greater labial displacement and an elevated risk of anchorage loss; in contrast, smaller step sizes preserved torque more effectively. Step size then amplified this effect—greater increments further promoted labial tipping, particularly in the central incisors relative to the lateral ones.

Figure 3 thus demonstrates that anterior intrusion could be achieved while maintaining labial tipping within a physiologic range, but only under the combined conditions of a small step size and moderate occlusal force. Such an approach effectively avoided the risk of anterior anchorage loss.

2.3 Spatial Evolution of the Instantaneous Center of Rotation and Rotation Axis

Without occlusal force, the maxillary canine underwent primarily tipping movement. The ICR resided near the root apex, far below the center of resistance (CRes) in the middle third of the root. This pattern showed that the clear aligner solely delivered an unbalanced force concentrated at the crown.

As occlusal force increased, the ICR shifted occlusally along the tooth's long axis, making the rotation axis increasingly horizontal and driving the motion from tipping toward near-bodily movement. When the applied force exceeded a critical threshold, the ICR shifted toward infinity, indicating that the tooth had entered a state of near-pure translation (rotation angle approaching 0°)[20].

The step size influenced this transition and interacted with occlusal force in a nonlinear manner (summarized in Table 2). For example, under a small step (0.10 mm), the ICR relative to CRes evolved with load as follows: from +5.25 mm at 0 N to −3.78 mm at 25 N, then to +0.52 mm at 50 N, and finally to +10.58-15.13 mm at 75–100 N. These data showed a continuous shift from tipping to root movement and finally to controlled translation.

We found that the 25–50 N induced the most pronounced shift of the ICR, indicating that under a small step size the system was highly sensitive to force magnitude at low thresholds. Contrastly, when using the largest step (0.25 mm), the ICR was initially located occlusal to CRes (h = +2.24 mm at 0 N). As the occlusal load rose to 100 N, it migrated apically to h = −4.58 mm, yet remained confined to the apical region. Notably, although the rotation axis angle (θ) decreased from 0.28° to 0.18°, an inertial locking effect emerged, likely because the excessive initial tipping moment prevented full transition to translation. The intermediate step sizes (0.15–0.20 mm) showed a transitional pattern between these two extremes.

Table 2. Projection height and rotation angle of maxillary canine ICR along the long axis of the tooth under different working conditions (CRes located at h = −2.0 mm / middle 1/3 of the root; h > 0 indicates ICR is occlusal to the centroid, h < −2 indicates ICR is apical to CRes)

Moving Step	Parameter	0 N	25 N	50 N	75 N	100 N
0.10 mm	h (mm)	5.25	−3.78	0.52	10.58	15.13
	Angle (°)	0.10	0.08	0.08	0.10	0.13
0.15 mm	h (mm)	3.39	−3.44	−1.80	5.08	9.87
	Angle (°)	0.16	0.14	0.15	0.18	0.23
0.20 mm	h (mm)	2.58	−1.36	−4.65	−0.92	3.60
	Angle (°)	0.22	0.19	0.19	0.22	0.25
0.25 mm	h (mm)	2.24	1.90	−1.13	−3.63	−4.58
	Angle (°)	0.28	0.24	0.22	0.19	0.18

As shown in Figure 4, three-dimensional analysis in the frontal, lateral, and occlusal views reveals that the movement occurs mostly in the sagittal and coronal planes, with negligible vertical rotation. On the occlusal view, the ICR translates linearly along the long axis of the tooth, showing no buccolingual or mesiodistal deviation.

Figures 5B and 5C quantify how ICR projection height and rotation angle change under load. Two anatomical references anchor the analysis: the CRes line (h = −2.0) and the centroid line (h = 0). The 0.10 mm group exhibited a characteristic "V-shaped rebound" in the ICR trajectory: a brief apical dip at 25 N, succeeded by a sharp coronal rebound and corresponding to controlled translation. In contrast, the 0.25 mm group showed a monotonic apical shift, with the ICR remaining confined to the apical region. Regarding rotation angles, θ remained below 0.3° across all loading conditions. In the 0.25 mm group, θ decreased from 0.28° to 0.18° as force increased. This indicates that, even when the ICR remained confined to the apical region, higher occlusal force effectively mitigated the unwanted rotation induced by aligner deformation.

Figures 5B and 5C show how ICR projection height and rotation angle change under load. The analysis uses two anatomical references: the CRes line (h = −2.0) and the centroid line (h = 0). In the 0.10 mm group, the ICR showed a characteristic V-shaped rebound — a brief apical dip at 25 N followed by a sharp coronal rebound, consistent with controlled translation. In contrast, the 0.25 mm group shifted monotonically apically, with the ICR remaining confined to the apical region throughout.

As for rotation angles, θ remained below 0.3° under all loads. In the 0.25 mm group, θ decreased from 0.28° to 0.18° as force increased. Thus, even with the ICR pinned to the apex, higher occlusal force obviously reduced the unwanted rotation caused by aligner deformation.

Discussion

FEA was first applied to orthodontics by Thresher et al. in 1973 [21,22] and has since been established as a key approach for simulating how the tooth–periodontal ligament–bone complex responds mechanically. In the present study, we built a computational model that discretized the maxillary incisors, supporting tissues, and the clear aligner to simulate displacement patterns and stress distributions under defined loading conditions[23]. This approach is especially valuable for addressing tricky clinical scenarios—such as extraction space closure, root control, and vertical adjustment—as it provides a theoretical basis for optimizing aligner mechanics and tailoring treatment plans[13,24].

The maxillary flat bite plate—typically bonded to the lingual surface of the incisors or canines—is a common device for bite opening in clear aligner extraction cases. When managing moderate to severe deep overbite that involves substantial anterior retraction or high torque demands, we extended the bite plate coverage to both canines. This eliminated the occlusal interference that maintains the deep bite lock, thereby creating the space needed for bite opening, anterior retraction, and mandibular repositioning[25].

The experimental data showed that combining a canine lingual bite plate with occlusal force converted distal canine movement from tipping toward bodily movement. We applied occlusal forces from 25 N to 100 N—spanning light to heavy biting [15]. FEA showed that under appliance-only activation (0 N), the ICR sat near the root apex, producing crown-distal and root-mesial tipping. Adding a vertical upward occlusal

force shifted the rotation axis; at certain force levels, it ran nearly parallel to the tooth's long axis — consistent with bodily translation. The vertical component counteracted the torque generated by aligner deformation, synchronizing crown and root distalization. Higher occlusal forces induced controlled root overcorrection — that is, root displacement exceeded crown displacement.

A notable issue with the largest step size (0.25 mm) was the "inertial locking" effect. Even a 100 N occlusal force could not overcome the initial tipping torque induced by aligner deformation, restricting the type of tooth movement. This highlights a clinical limitation: high-intensity biting alone cannot fully offset the mechanical constraints of an excessively large step size.Our model suggests that forces over 75 N may facilitate better root control, but clinical application warrants caution. Considering the gap between simulated peak forces and patients' actual occlusal forces, we recommend moderate forces (25–50 N per side) combined with active bite training during treatment. This strikes a reasonable balance between periodontal safety and effective tooth movement.

Using the flat guide plate to alter canine movement also introduced unintended effects on the anterior segment. In conventional clear aligner treatment for extraction cases, inadequate vertical and torque control often leads to a "roller coaster pattern"—characterized by lingual tipping and extrusion of the anterior teeth[13,26,27]. Our results showed that the canine bite ramp improved root control during distalization. The transmitted occlusal force also induced vertical intrusion while producing labial tipping of the incisors, thereby partly counteracting the undesired effect[28]. However, this compensatory mechanism proved double-edged. Excessive occlusal force (≥ 75 N) or step size (≥ 0.20 mm) exacerbated incisor labial tipping, potentially compromising anterior anchorage—a risk consistent with prior observations of proclination in clear aligner treatment[29]. Conversely, reducing the step size improved predictability, and enabled more controlled tooth movement. Thus, clinicians must strike a balance: counteracting the roller coaster effect while avoiding excessive labial tipping of the incisors.

We simulated four movement step sizes (0.10, 0.15, 0.20, and 0.25 mm) to evaluate how step size affects the mechanical environment. The 0.10 mm step performed best: it required less occlusal force to achieve the same bodily translation and also systematically reduced incisor labial tipping. Our analysis suggests that smaller steps reduce the initial interference between the aligner and the tooth, making force delivery more predictable. Importantly, the intermediate step sizes represent a practical compromise between the efficiency of the conventional 0.25 mm step and the biological control offered by the 0.10 mm step. Clinicians should therefore tailor step size across different treatment phases, weighing efficiency against periodontal safety.

Our FEA models showed that the canine lingual bite plate promoted bodily movement during canine distalization, and the effect got stronger as we increased occlusal force. Smaller steps reduced unwanted incisor flaring and helped maintain anterior anchorage. Because this was a computational simulation, certain factors — dynamic occlusion, salivary dynamics, periodontal biological responses — lie beyond what FEA models can simulate. Clinical validation is needed to confirm whether these biomechanical trends hold true across different malocclusion types and attachment configurations.

Abbreviations

CBR: Canine Bite Ramp

ICR: Instantaneous Center of Rotation

CBCT: Cone Beam Computed Tomography

PCA: Principal Component Analysis

CRes: Center of Resistance

Declarations

Ethics approval and consent to participate

This study was conducted in accordance with the ethical principles of the Declaration of Helsinki and approved by the Ethics Committee of the Affiliated Stomatological Hospital of Nanjing Medical University (Approval No. NKYEC-PJ2023-163-001). Written informed consent for publication of clinical data and images was obtained from the patient's parents/legal guardians.

Consent for publication

Not applicable.

Availability of data and materials

The datasets used and/or analysed during the current study are available from the corresponding author on reasonable request.

Competing interests

The authors declare that they have no known competing financial interests or personal relationships that could have appeared to influence the work reported in this paper.

Funding

This work was supported by the Open Project of National Key Laboratory of Oral Disease Research and Prevention in Nanjing Medical University (JSKLOD-KF-2502) and the Natural Science Foundation of Jiangsu Province (BK20210529).

Authors' contributions

JW and YC performed the finite element analysis and drafted the manuscript. YZ and KZ assisted with model construction and data interpretation. GL contributed to the biomechanical design. CZ and ZY

conceived the study, supervised the research, and revised the manuscript. All authors read and approved the final manuscript.

Acknowledgements

Not applicable.

References

1. Gao M, Yan X, Zhao R, et al. Comparison of pain perception, anxiety, and impacts on oral health-related quality of life between patients receiving clear aligners and fixed appliances during the initial stage of orthodontic treatment. European J Orthod Jun. 2021;8(3):353–9.
2. Wang YG, Zhu GY, Liu JQ, Wang YF, Zhao ZH. Dynamic biomechanical changes of clear aligners during extraction space closure: Finite element analysis. American J Orthod Dentofac orthopedics: official publication Am Association Orthodontists its constituent Soc Am Board Orthod Mar. 2024;165(3):272–e284273.
3. Al-Nadawi M, Kravitz ND, Hansa I, Makki L, Ferguson DJ, Vaid NR. Effect of clear aligner wear protocol on the efficacy of tooth movement. The Angle Orthod Mar. 2021;1(2):157–63.
4. Liu JQ, Zhu GY, Wang YG, Zhang B, Yao K, Zhao ZH. Different biomechanical effects of clear aligners in closing maxillary and mandibular extraction spaces: Finite element analysis. American J Orthod Dentofac orthopedics: official publication Am Association Orthodontists its constituent Soc Am Board Orthod Jun. 2023;163(6):811–e824812.
5. Qian Y, Tang Z, Chen Y et al. The 'roller coaster effect' in premolar extraction cases: clear aligners vs. straight-wire appliance. European J Orthod Dec 4 2024;47(1).
6. Zhu GY, Zhang B, Yao K, et al. Finite element analysis of the biomechanical effect of clear aligners in extraction space closure under different anchorage controls. American J Orthod Dentofac orthopedics: official publication Am Association Orthodontists its constituent Soc Am Board Orthod May. 2023;163(5):628–e644611.
7. Khosravi R, Cohanim B, Hujoel P et al. Apr. Management of overbite with the Invisalign appliance. *American journal of orthodontics and dentofacial orthopedics: official publication of the American Association of Orthodontists, its constituent societies, and the American Board of Orthodontics*. 2017;151(4):691–699.e692.
8. Al-Balaa M, Li H, Ma Mohamed A, et al. Predicted and actual outcome of anterior intrusion with Invisalign assessed with cone-beam computed tomography. American J Orthod Dentofac orthopedics: official publication Am Association Orthodontists its constituent Soc Am Board Orthod Mar. 2021;159(3):e275–80.
9. Wang S, Peng X, Tian Z, Wang Y, Zhou Y. Canine distal movement impact on teeth and aligner deformation in clear aligner treatment: A 3D finite element study. Journal World federation orthodontists Jan 28 2026.

10. Baek SE, Kim K, Choi YK, et al. Effects of clear aligner edentulous space design on distal canine movement: An iterative finite element analysis in cases involving extraction. Korean J Orthod May. 2025;25(3):193–201.
11. Jain A, Prasantha GS, Mathew S, Sabrish S. Analysis of stress in periodontium associated with orthodontic tooth movement: a three dimensional finite element analysis. Computer methods Biomech biomedical Eng Dec. 2021;24(16):1841–53.
12. Ammar HH, Ngan P, Crout RJ, Mucino VH, Mukdadi OM. Three-dimensional modeling and finite element analysis in treatment planning for orthodontic tooth movement. American J Orthod Dentofac orthopedics: official publication Am Association Orthodontists its constituent Soc Am Board Orthod Jan. 2011;139(1):e59–71.
13. Liu L, Song Q, Zhou J, et al. The effects of aligner overtreatment on torque control and intrusion of incisors for anterior retraction with clear aligners: A finite-element study. American J Orthod Dentofac orthopedics: official publication Am Association Orthodontists its constituent Soc Am Board Orthod Jul. 2022;162(1):33–41.
14. Guerrero-Vargas JA, Montalvany-Antonucci CC, Velez-Muriel SM, Couto Figueiredo N, Macari S. Correction of the curve of spee using clear aligner therapy: A finite element analysis of three lower anterior intrusion protocols. PLoS ONE. 2026;21(1):e0341447.
15. Edmonds HM, Glowacka H. The ontogeny of maximum bite force in humans. Journal Anat Sep. 2020;237(3):529–42.
16. Yang Y, Pan S, Zhao J, Pan X, Tsai TY. Three-dimensional zone of the centers of resistance of the mandibular incisors and canines: A novel approach by finite element analysis. International Orthod Mar. 2025;23(1):100933.
17. de Arruda JAA, Colares JP, Santos MS et al. Studying Orthodontic Tooth Movement in Mice. Journal visualized experiments: JoVE Aug 2 2024(210).
18. Zheng X, Zhou T, Fan Y, et al. Reconstruction accuracy enhancement of fiber shape sensing by Kabsch-algorithm-based pose correction. Optics express Feb. 2026;23(4):7208–19.
19. Wechsler I, Shanbhag J, Wartzack S, Koelewijn AD, Miehling J. IMU-based joint axis identification method for arbitrary joints in OpenSim - a simulation study. BMC biomedical Eng Nov. 2025;21(1):16.
20. Owens SE, Buschang PH, Cope JB, Franco PF, Rossouw PE. Experimental evaluation of tooth movement in the beagle dog with the mini-screw implant for orthodontic anchorage. American J Orthod Dentofac orthopedics: official publication Am Association Orthodontists its constituent Soc Am Board Orthod Nov. 2007;132(5):639–46.
21. Elshazly TM, Bourauel C, Aldesoki M, et al. Computer-aided finite element model for biomechanical analysis of orthodontic aligners. Clinical oral investigations Jan. 2023;27(1):115–24.
22. Thresher RW, Saito GE. The stress analysis of human teeth. Journal Biomech Sep. 1973;6(5):443–9.
23. Yang PZ, Bai LY, Zhang HX, et al. Efficacy of a four-curvature auxiliary arch at preventing maxillary central incisor linguoclination during orthodontic treatment: a finite element analysis. BMC oral

health Mar. 2023;11(1):144.

24. Cozzani M, Sadri D, Nucci L, Jamilian P, Pirhadirad AP, Jamilian A. The effect of Alexander, Gianelly, Roth, and MBT bracket systems on anterior retraction: a 3-dimensional finite element study. Clinical oral investigations Mar. 2020;24(3):1351–7.
25. Kou B, Xu Y, Liu Q et al. The effect of bite planes on deepbite correction with clear aligners. Clinical oral investigations May 16 2026;30(6).
26. Alsawaf DH, Rajah N. Evaluation of efficacy of utility arch with inter-maxillary elastics for treating skeletal deep bite with retroclined upper incisors in the mixed dentition: a clinical randomized controlled trial. The Angle Orthod May. 2023;1(3):296–305.
27. Pang H, Che X. CBCT analysis of mandibular position and bilateral symmetry in adult female patients with a deep overbite before and after flat bite plate treatment: a retrospective study. European J Med Res Nov. 2024;16(1):551.
28. Nucera R, Dolci C, Bellocchio AM et al. Effects of Composite Attachments on Orthodontic Clear Aligners Therapy: A Systematic Review. Materials (Basel Switzerland) Jan 11 2022;15(2).
29. Kang F, Wu Y, Cui Y, Yuan J, Hu Z, Zhu X. The displacement of teeth and stress distribution on periodontal ligament under different upper incisors proclination with clear aligner in cases of extraction: a finite element study. Progress Orthod Nov. 2023;20(1):38.

Figures

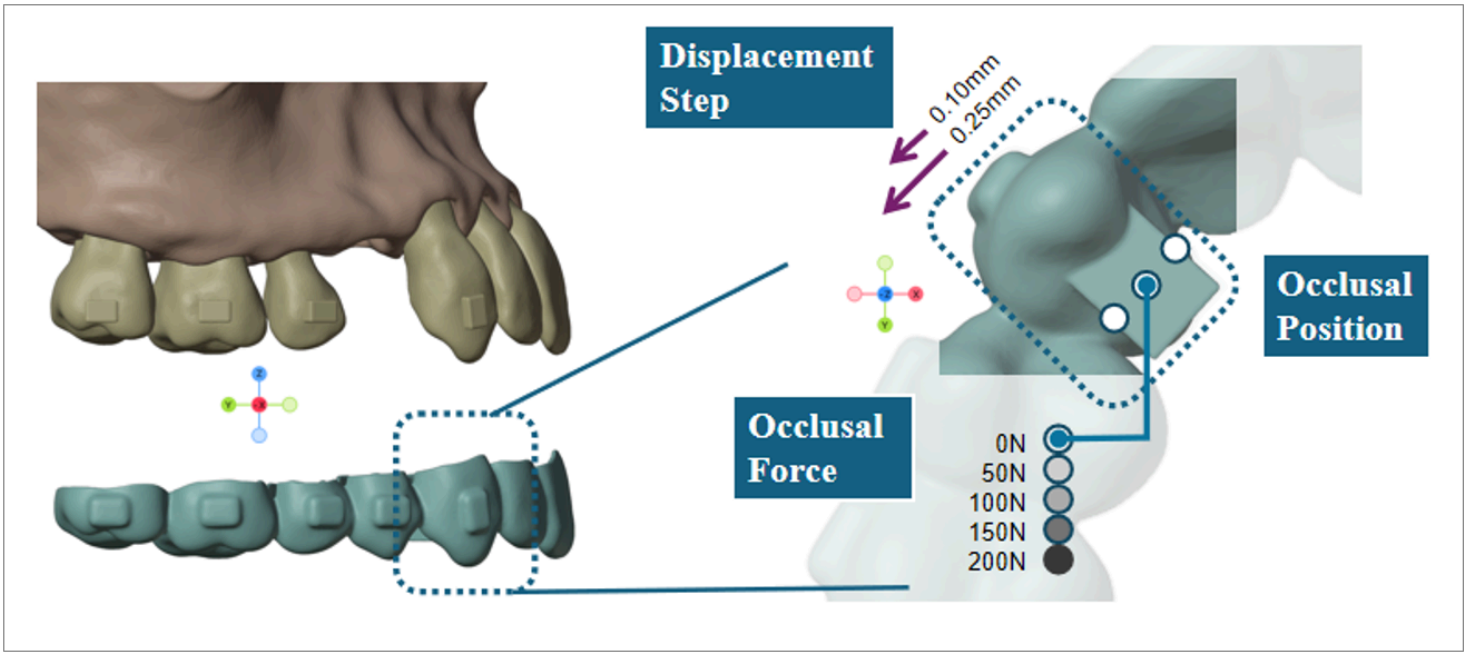


Figure 1

Experimental design

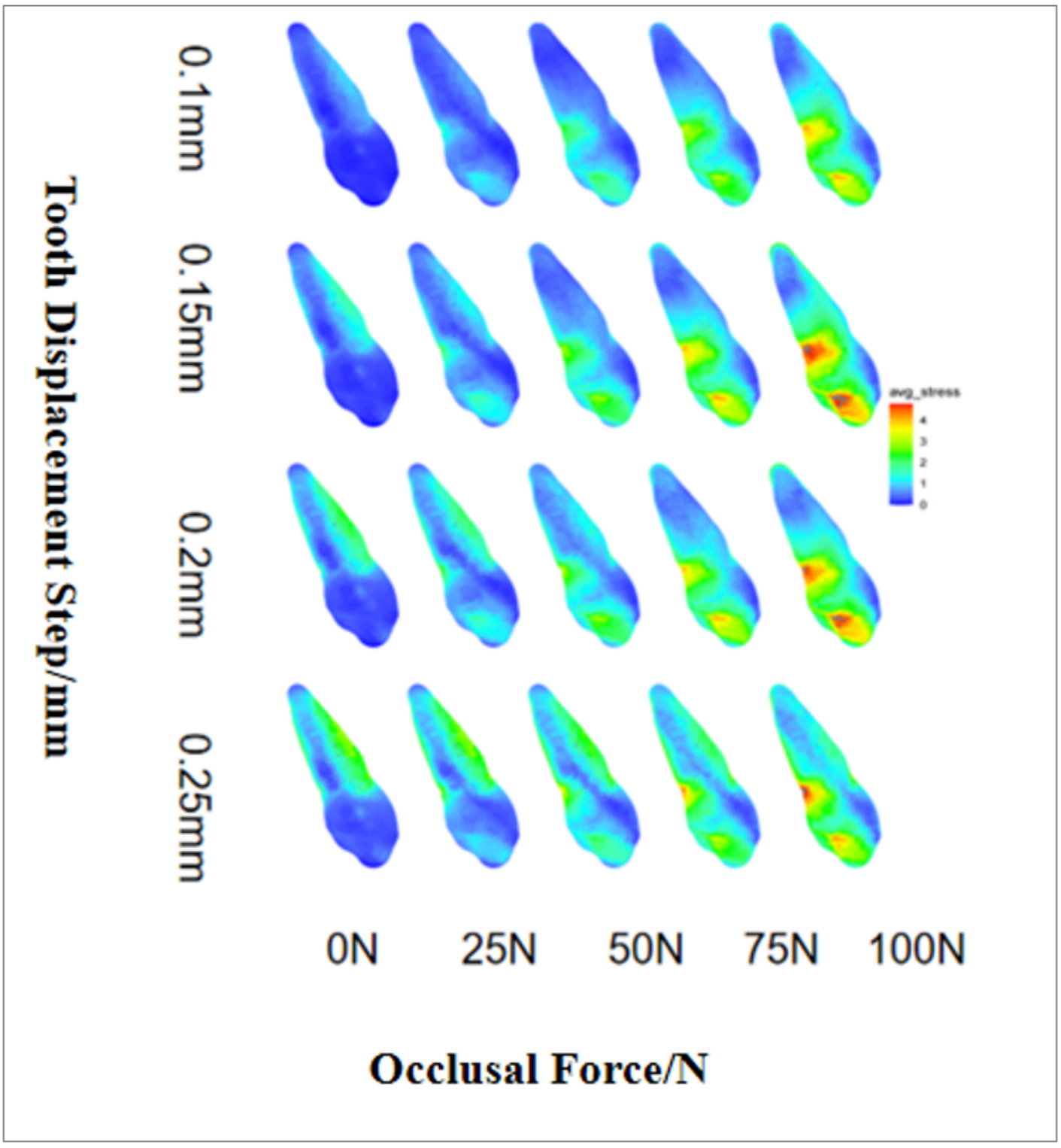


Figure 2

Von-Mises stress distribution on the lingual surface of maxillary canines under varying occlusal forces and movement strides

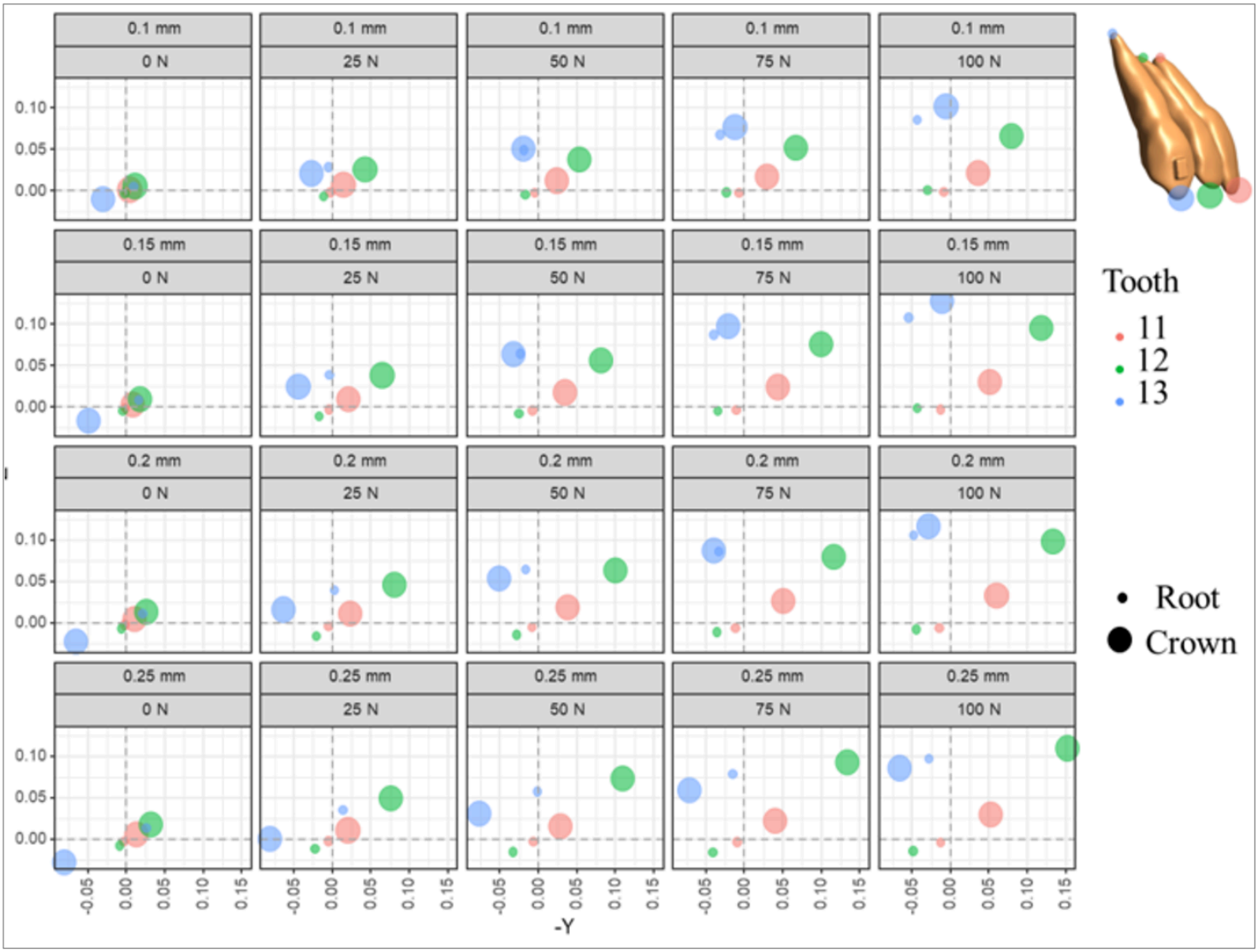


Figure 3

Displacement distribution of maxillary anterior tooth crowns and root apices under different conditions (Y-axis: horizontal displacement, positive → mesial / negative → distal; Z-axis: vertical displacement, positive → extrusion / negative → intrusion; unit: mm).

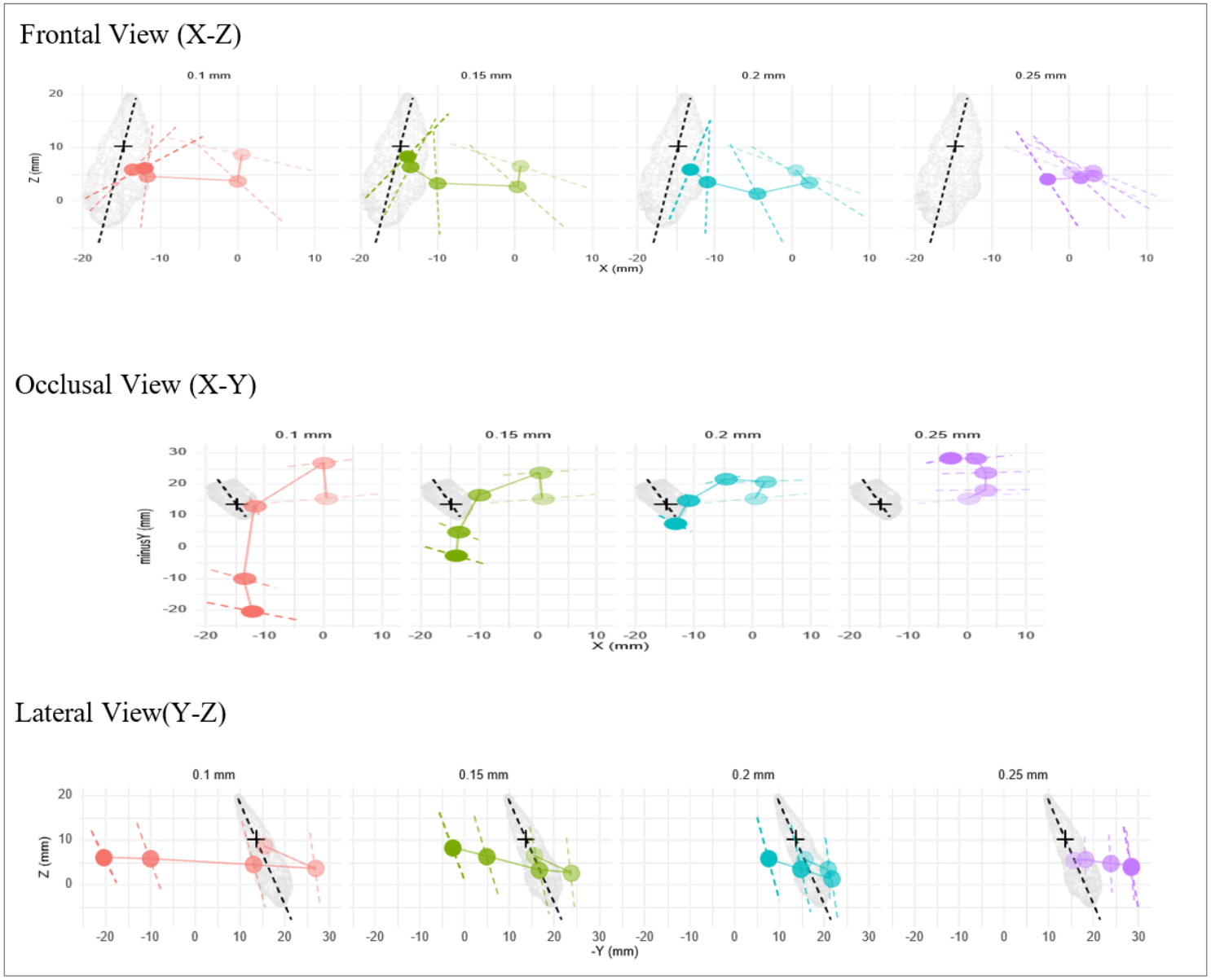


Figure 4

3D visualization of maxillary canine ICR and rotation axis under varying occlusal forces and movement steps. (Gray outline: canine shape; black dashed line: tooth long axis/PC1; black cross: CRes; colored dots: ICR under each condition; colored line segments: corresponding instantaneous rotation axis.)

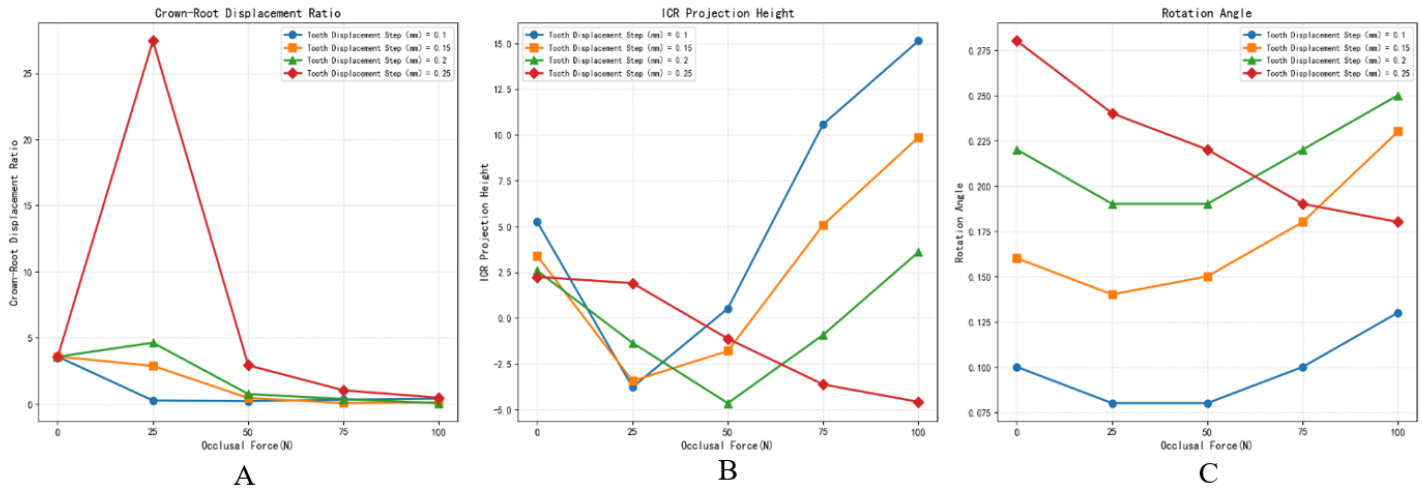


Figure 5

Line charts of quantitative indicators under increasing occlusal force. (A) Crown-root displacement ratio; (B) ICR projection height; (C) Rotation angle.